Available online at www.sciencedirect.com
ScienceDirect
Advances in Space Research 46 (2010) 174–179
ADVANCES IN SPACE RESEARCH (a COSPAR publication)
www.elsevier.com/locate/asr

Estimated errors in a global gravity wave climatology from GPS radio occultation temperature profiles

A. de la Torre [a,*], P. Llamedo [a,1], P. Alexander [b,2], T. Schmidt [c], J. Wickert [c,3]

[a] Facultad de Ingeniería, Universidad Austral, Av. Garay 125, C1063ABB Buenos Aires, Argentina
[b] Departamento de Física, Facultad de Ciencias Exactas y Naturales, Universidad de Buenos Aires, Ciudad Universitaria, 1428 Buenos Aires, Argentina
[c] Helmholtz Centre Potsdam, GFZ German Research Centre for Geosciences, Telegrafenberg A17, Potsdam, D-14473, Germany

Received 8 September 2009; received in revised form 24 February 2010; accepted 25 February 2010

Abstract

In a previous paper by Schmidt et al. (2008), from CHAllenging Minisatellite Payload (CHAMP) Global Positioning System (GPS) radio occultation data, a comparison was made between a Gaussian filter applied to the "complete" temperature profile and to its "separate" tropospheric and stratospheric height intervals, for gravity wave analyses. It was found that the separate filtering method considerably reduces a wave activity artificial enhancement near the tropopause, presumably due to the isolation process of the wave component. We now propose a simple approach to estimate the uncertainty in the calculation of the mean specific wave potential energy content, due exclusively to the filtering process of vertical temperature profiles, independently of the experimental origin of the data. The approach is developed through a statistical simulation, built up from the superposition of synthetic wave perturbations. These are adjusted by a recent gravity wave (GW) climatology and temperature profiles from reanalyses. A systematic overestimation of the mean specific wave potential energy content is detected and its variability with latitude, altitude, season and averaging height interval is highlighted.

Keywords: Gravity waves; Wave energy; GPS radio occultation

1. Introduction

The importance of atmospheric waves in the transport of vertical and horizontal momentum and energy across the lower and middle atmosphere was recognized at an early stage (*e.g.* Jin et al., 2008, 2009). Many experimental efforts, accomplished during the last two decades, gave rise to a fruitful budget of rocket, radar, lidar, aircraft and radiosonde data (*e.g.* Tsuda et al., 1991; Nastrom and Fritts, 1992; Fritts and Nastrom, 1992; Senft et al., 1993; Eckermann and Vincent, 1993; Eckermann et al., 1995; Allen and Vincent, 1995; Wu and Waters, 1996). Limb and nadir sounding instruments on board of different satellites later extended the limited spatial coverage provided by ground and on-site based devices (*e.g.* Tsuda et al., 2000; Ratnam et al., 2004; Alexander et al., 2008a, in press; Kawatani et al., 2009). All the main advantages and weaknesses of each sounding device to detect wave parameters, their associated forbidden spectral range, characteristic inertial frame of observation, etc., have been extensively pointed out (e.g. Alexander, 1998; Wu et al., 2006; de la Torre et al., 2006; Ern et al., 2008).

When experimental temperature $T(z)$ data of whatever origin (radiosoundings, GPS radio occultation (RO), etc.), are processed for global wave analyses, the mean specific (per unit mass) potential energy content between height altitudes z_1 and z_2, is calculated as

* Corresponding author. Tel.: +54 11 5921 8000x8503; fax: +54 11 5921 8000x8342.
E-mail addresses: Adelatorre@austral.edu.ar (A. de la Torre), Pllamedo@austral.edu.ar (P. Llamedo), peter@df.uba.ar (P. Alexander), tschmidt@gfz-potsdam.de (T. Schmidt), wickert@gfz-potsdam.de (J. Wickert).
[1] Tel.: +54 11 5921 8000x8503; fax: +54 11 5921 8000x8342.
[2] Tel.: +54 11 4576 3390x804; fax: +54 11 4576 3357.
[3] Tel.: +49 331 2881743/+49 331 2881758; fax: +49 331 2881732.

0273-1177/$36.00 © 2010 COSPAR. Published by Elsevier Ltd. All rights reserved.
doi:10.1016/j.asr.2010.02.033

$$E_P = \frac{1}{2(z_2 - z_1)} \int_{z_1}^{z_2} \frac{g^2}{N^2(z)} \left[\frac{T'(z)}{T(z)}\right]^2 dz, \quad (1)$$

where T', g and N are the perturbation component, the acceleration of gravity and the buoyancy frequency. This variable represents a general indication of atmospheric wave activity (WA) (*e.g.* de la Torre et al., 2006; Alexander et al., in press), by allowing to develop realistic GW analyses from $T'(z)$ data alone, after separating $T'(z)$ from the background $T(z)$ vertical profiles. Nevertheless, this WA indication and the generally accepted uniform partition assumption between potential and kinetic wave energy, have some restrictions at midlatitudes, where the jet stream often has its maximum speed at the tropopause level. It is suspected that the tropopause may influence mountain waves propagating into the stratosphere. The sharp lapse rate and wind shear change at the tropopause may cause partial reflection and discontinuous aspects of wave structure (Smith et al., 2008).

1.1. Alternative methods in the processing of vertical temperature profiles

As Schmidt et al. (2008) (*SCH08*) pointed out, when the spatial and temporal measurement density is sufficient, the determination of a background temperature by averaging over appropriate latitude/longitude and time bins is possible. This may be the case when, for example, RO COSMIC (Constellation Observing System for Meteorology, Ionosphere and Climate) data are processed (Alexander et al., in press). These authors constructed for each grid cell a background T and pressure profile over a 7-day interval, obtaining vertically averaged means. The oscillation components were obtained by subtracting individual raw T profiles from the appropriate background mean T. Then, they removed any vertical linear trend before Welch windowing. Finally a 7 km highpass filtering was applied.

On the other hand, the number of profiles per bin may be scanty to generate representative average T backgrounds. This is the case with the long-term CHAMP GPS RO data set analyzed by *SCH08* and de la Torre et al. (2006) (and every previous global radiosonde data analysis). Here, a different method, suitable to extract the wave component from each single T background profile, needs to be applied. This wave component may be calculated after extracting the perturbation component from each single T profile, by applying a band-pass filter (*e.g.* Eckermann et al., 1995; Tsuda et al., 2000). It should be stressed here that the uncertainty in the calculation of E_P exclusively due to this filtering process must be considered independently of additional errors during the retrieval. These were detailed for example in Alexander et al. (2008b): amplitude attenuation and phase shifts, departures from spherical symmetry in the background atmosphere due to the waves, wave fronts orientation relative to lines of sight, etc. A different approach (*e.g.* Allen and Vincent, 1995) obtained normalized temperature fluctuation profiles by estimating the mean T with a fitted second-order polynomial over the height interval under study.

Regarding Eq. (1), the WA could be calculated as an average in time or space along any possible horizontal, vertical or even slanted directions. Each option will be affected by its own weaknesses (e.g. Alexander et al., 2008b).

The tropopause abrupt change in the T lapse rate restricted previous GW analyses to height intervals beginning around 1 or 2 km above the tropopause. Nevertheless, *SCH08* analyzed WA including the tropopause region. They applied a Gaussian filter both to the "complete" temperature profile and to "separate" tropospheric and lower and middle stratospheric height intervals. The complete method, ideally, would allow for the detection of longer wavelengths than the separate one. Besides providing an updated global description of WA distribution, these authors emphasized three main conclusions: (i) the separate filtering method considerably reduces, as expected, the WA enhancement due to the tropopause effect; (ii) except within 3 km around the lapse rate tropopause (LRT), both methods deliver identical normalized T fluctuations; and (iii) a statistical quantification of the overall under- or overestimation of WA at the tropopause is crucial.

Regarding the last point, we assume that it is not possible to accurately extract each perturbation component from each raw T profile. On the other hand, we also considered the possibility to calculate WA in the troposphere–stratosphere system from other parameters. We observed very similar enhancements in WA (contrarily to what we expected) at the tropopause region, using temperature or potential temperature profiles. Below, we propose an approach to estimate the uncertainty generated during the filtering process in the calculation of the mean WA from T profiles. This uncertainty is expressed as a function of latitude, altitude and height interval of WA averaging.

2. Synthetic vertical temperature profiles

We create synthetic T data between 4 and 27 km height, by adding a background component T_B plus a perturbation T'. These known profiles provide us with a reference value of E_P. This in turn will be compared with the processed T profiles, after applying the complete and separate filtering methods described above.

We proceed as follows:

(1) T_B is selected from NCEP reanalyses data, at intervals of 5° latitude, zonally averaged and randomly chosen between January 1997 and December 2007 (the maximum common height interval available for every latitude and time is 4–27 km).
(2) T' is generated as a superposition of monochromatic waves with vertical wavelengths λ_j ranged between 1.0 and 15.0 km every 0.5 km.

$$T'(z) = \sum_{j=1}^{29} A_j sin\left(\frac{2\pi}{\lambda_j} z + \phi\right) \quad (2)$$

where A_j and ϕ are random numbers for amplitude and phase, respectively.

In order to make the generated T' profiles compatible with climatological evidence, we derive a modulation function f that matches T' to recent GPS RO long-term global observations, as shown in *SCH*08. The f function is calculated as follows:

$$f = \frac{D[T'_{SCH08}(z,lat)]}{\frac{1}{N}\sum_{i=1}^{N} D[T'_i(z)]} = \frac{D[T'_{SCH08}(z,lat)]}{\frac{1}{N}\sum_{i=1}^{N}\sum_{j=1}^{29} D\left[A_j sin\left(\frac{2\pi}{\lambda_j}z+\phi\right)\right]} \quad (3)$$

where D is an envelope function, only included to avoid possible zeroes arising in the denominator when f is derived. The f function depends on latitude and height. Then T' as generated in (2) is multiplied by f. The resulting perturbation basically reproduces the traditional theoretical spectral slope $\propto k_z^{-3}$ for GW fluctuations, largely discussed and tested against experimental data by several authors (e.g. Smith et al., 1987; VanZandt et al., 1990; de la Torre et al., 1994) (not shown).

3. Error distribution in E_P due to the filtering process

Each synthetic T profile, created as explained above, is band-pass filtered using the complete and separate method, with an upper cutoff of 15.0 km. Both methods yield different separations between background and perturbation, respectively:

$$T = T_B^C + T'^C = T_B^S + T'^S \quad (4)$$

After deriving $N^2(z,lat)$, we distinguish between the reference wave potential energy E_P^{REF} and those calculated using the complete and separate filtering methods, E_P^C and E_P^S:

$$E_P^{REF}(z,lat) = \frac{1}{2(z_2-z_1)}\int_{z_1}^{z_2}\left(\frac{g}{N^{REF}(z)}\right)^2\left[\frac{T'(z,lat)}{T_B(z,lat)}\right]^2 dz \quad (5)$$

and

$$E_P^{C,S}(z,lat) = \frac{1}{2(z_2-z_1)}\int_{z_1}^{z_2}\left(\frac{g}{N^{C,S}(z)}\right)^2\left[\frac{T'^{C,S}(z,lat)}{T_B^{C,S}(z,lat)}\right]^2 dz \quad (6)$$

respectively. Here, $z=(z_1+z_2)/2$ and $\Delta z = z_2 - z_1$ is constant.

For each latitude, we analyze 10^4 profiles with the complete and separate method. At this point, we checked that any number of profiles above around 500 per latitude, produce identical results. The relative error for each profile is calculated as:

$$\epsilon_i^R = \left[E_P^{REF}(z,lat) - E_P^{C,S}(z,lat)\right]/E_P^{REF}(z,lat) \quad (7)$$

where the sign is retained. Finally, after averaging over each ensemble, $\epsilon^R(z,lat)$ is obtained.

4. Results

The climatology for $E_P(z,lat)$ as shown by *SCH08* from CHAMP data, here extended to September 2008, for the complete and separate method, is shown in Fig. 1a–b. *SCH08* considered $\Delta z = 2$ km. In Fig. 1c to h, $\epsilon^R(z,lat)$ is shown comparatively for $\Delta z = 2,\ 5$ and 10 km, also for the complete and separate method. Given these selected intervals and synthetic profiles between 4 and 27 km, the results for each sliding window are available in the following altitude ranges: 5.0–26.0 km, 6.5–24.5 km and 9.0–22.0 km, respectively.

The estimated errors, following the usual definition for $\epsilon^R(z,lat)$ in (7), were obtained under the hypothesis that the "true" value is equal to the "reference" value. The maximum $\epsilon^R(z,lat)$ values may be found to be unexpectedly large. The following features may be pointed out: (i) an overall overestimation of $E_P(z,lat)$ with both methods, expressed in terms of ϵ^R for any selected Δz; (ii) ϵ^R exhibits general decreasing values with increasing Δz, (iii) ϵ^R, as expected, is considerably more significative around the tropopause with the complete method; (iv) away from the tropopause region, the minima of ϵ^R are mainly situated in the troposphere and, in the stratosphere, except at high latitudes in SH (Southern Hemisphere) and in two narrow regions centered around +40 and −40°. Finally, in Fig. 1i–l we show the seasonal behavior of ϵ^R for $\Delta z = 2$ km (this is not appreciated in Fig. 1c–d). Here we consider separately only background profiles from December, January, February (DJF) and June, July, August (JJA), for the complete and separate methods, respectively. Besides minor features, a clear enhancement of ϵ^R at high latitudes during summer in NH (Northern Hemisphere) due to the considerable dispersion of stratospheric lapse rates in T_B profiles is observed. This feature is not present during winter; however, the annually mean increased ϵ^R values in this region in Fig. 1c–d are thus explained.

Note that if we extract E_P^{REF} from

$$\epsilon^R = \left[E_P^{REF}(z,lat) - E_P^{C,S}(z,lat)\right]/E_P^{REF}(z,lat) \quad (8)$$

we may check that, replacing results from Fig. 1c and d and adding C, S indexes, the difference

$$\Delta = \frac{E_P^C}{1-\epsilon^{R,C}} - \frac{E_P^C}{1-\epsilon^{R,S}} \quad (9)$$

vanishes, as expected (not shown). This was checked also for every remaining pair of left and right side Fig. 1(e,g,i,k–1f,h,j,l), respectively.

To better appreciate these features, ϵ^R at two representative constant altitudes: 20 and 10 km, for $\Delta z = 2,\ 5$ and 10 km, is shown in Fig. 2a–b. We underline here: (i) the overall more accurate estimation of E_P with the separate method (mainly in NH) as well as with increasing Δz, and (ii) the extreme minimum in ϵ^R in the troposphere at low latitudes.

5. Conclusions

We propose a simple method based on the random generation of synthetic data to estimate possible uncertainties

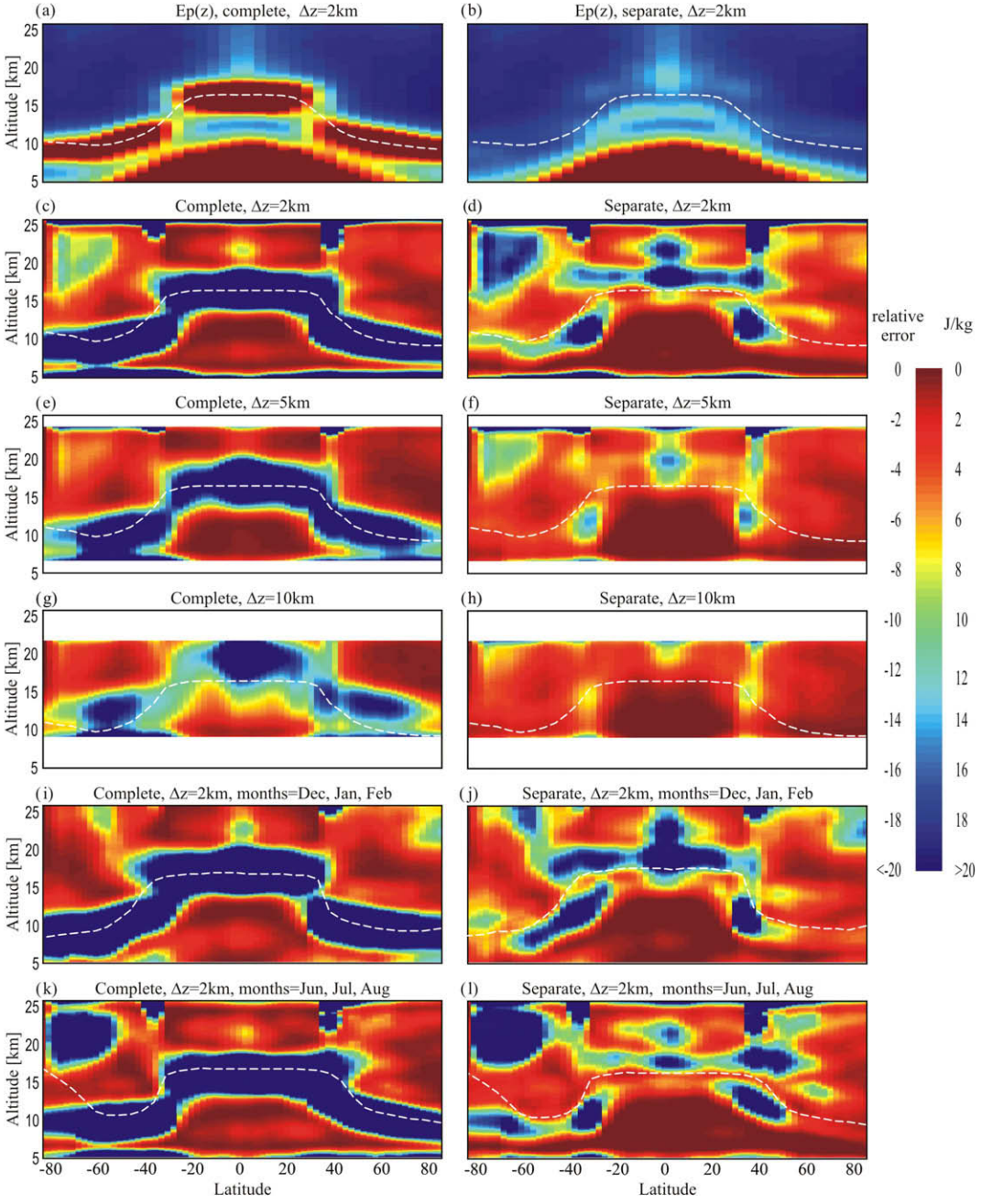

Fig. 1. Climatology for $E_P(z, lat)$ as shown by SCH08, extended to September 2008, for the (a) complete and (b) separate method, ($\Delta z = 2$ km).$\epsilon^R(z, lat)$ for $\Delta z = b - c$) 2, (d–e) 5 and (f–g) 10 km. Due to these selected intervals, results are available at the altitude ranges: 5.0–26.0, 6.5–24.5 and 9.0–22.0 km, respectively. (i–l) Seasonal behavior of ϵ^R for $\Delta z = 2$ km (not appreciated in c–d).

in the calculation of a climatology of mean specific wave potential energy content. The errors considered are only attributable to the processing of individual T profiles and not to the retrieval process itself. Under the hypothesis that the "true" value for E_P is identical to its "reference" value, the results suggest a systematic overestimation when a low-pass filter to each raw T profile is applied to remove the background component. This method was independently applied to each complete profile and to two separate consecutive intervals of it, above and below the LRT respectively. An overall global overestimation of E_P, with relative estimated errors ranging between −0.2 down to extremely low values, is observed. The separate method allows for better overall accuracy, mainly in the troposphere and in NH stratosphere. This accuracy is enhanced during winter in NH and specially, as the selected interval for integration in E_P is chosen progressively longer than 2 km, approaching the total energy content (between 4 and 27 km – not shown here –).

We assume that the processing of individual T profiles may be reasonably applied independently of the available density of T profiles (CHAMP as well as COSMIC RO

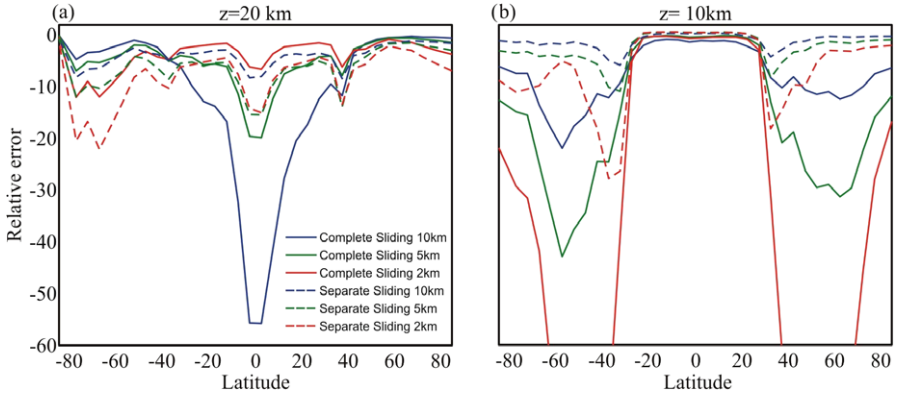

Fig. 2. ϵ^R at three representative constant altitudes: (a) 20 and (b) 10 km, for $\Delta z = 2,\ 5$ and 10 km.

data). An approach to an estimation of the possible uncertainties associated to the method mentioned in Section 1.1, based on the determination of a background temperature by averaging over appropriate latitude/longitude and time bins, is under study.

Acknowledgements

Manuscript prepared under grants UBA X004, CONICET PIP 5932 and ANPCyT PICT 1999. A. de la Torre and Alexander are members and P. Llamedo holds a fellowship of CONICET. The GFZ contribution was partially funded through DFG priority program CAWSES SPP 1176. We acknowledge data provided by the NOAA-CIRES/Climate Diagnostics Center, Boulder (CO) from their website www.cdc.noaa.gov.

References

Alexander, M.J. Interpretations of observed climatological patterns in stratospheric gravity wave variance. J. Geophys. Res. 103 (D8), 8627–8640, 1998.

Alexander, M.J., Gille, J., Cavanaugh, C., et al. Global estimates of gravity wave momentum flux from high resolution dynamics limb sounder observations. J. Geophys. Res. 113, D15S18, doi:10.1029/2007JD008807, 2008a.

Alexander, P., de la Torre, A., Llamedo, P. Interpretation of gravity wave signatures in GPS radio occultations. J. Geophys. Res. 113, D16117, doi:10.1029/2007JD009390, 2008b.

Alexander, P.A., Tsuda, T., Kawatani, Y., Takahashi, M. Global distribution of atmospheric waves in the equatorial upper troposphere and lower stratosphere: COSMIC observations of wave mean flow interactions. J. Geophys. Res., oi:10.1029/2008JD010039.

Allen, S.J., Vincent, R.A. Gravity wave activity in the lower atmosphere: seasonal and latitudinal variations. J. Geophys. Res. 100 (D1), 1327–1350, 1995.

de la Torre, A., Giraldez, A., Alexander, P. Saturated gravity wave spectra measured with balloons in Mendoza (Argentina). Geophys. Res. Lett. 21, 2039–2042, 1994.

de la Torre, A., Schmidt, T., Wickert, J. A global analysis of wave potential energy in the lower stratosphere derived from 5 years of GPS radio occultation data with CHAMP. Geophys. Res. Lett. 33, L24809, doi:10.1029/2006GL027696, 2006.

Eckermann, S.D., Vincent, R.A. VHF radar observations of gravity-wave production by cold fronts over southern Australia. J. Atmos. Sci. 50, 785–806, 1993.

Eckermann, S.D., Hirota, I., Hocking, W.K. Gravity wave and equatorial wave morphology of the stratosphere derived from long-term rocket soundings. Q.J.R. Meteorol. Soc. 121, 149–186, 1995.

Ern, M., Preusse, P., Krebsbach, M., Mlynczak, M.G., Russell III, J.M. Equatorial wave analysis from SABER and ECMWF temperatures. Atmos. Chem. Phys. 8 (666), 845–869, 2008.

Fritts, D.C., Nastrom, G.D. Sources of mesoscale variability of gravity waves, II, Frontal, convective, and jet stream excitation. J. Atmos. Sci. 49, 111–127, 1992.

Jin, S.G., Wu, Y., Heinkelmann, R., Park, J. Diurnal and semidiurnal atmospheric tides observed by co-located GPS and VLBI measurements. J. Atmos. Solar Terr. Phys. 70 (10), 1366–1372, doi:10.1016/j.jastp.2008.04.005, 2008.

Jin, S.G., Luo, O., Gleason, S. Characterization of diurnal cycles in ZTD from a decade of global GPS observations. J. Geodesy 83 (6), 537–545, 2009.

Kawatani, Y., Takahashi, M., Sato, K., Alexander, S.P., Tsuda, T. Global distribution of atmospheric waves in the equatorial upper troposphere and lower stratosphere: AGCM simulation of sources and propagation. J. Geophys. Res. 114, D01102, doi:10.1029/2008JD010374, 2009.

Nastrom, G.D., Fritts, D.C. Sources of mesoscale variability of gravity waves, I, topographic excitation. J. Atmos. Sci. 49, 101–110, 1992.

Ratnam, M.V., Tetzlaff, G., Jacobi, C. Global and seasonal variations of stratospheric gravity wave activity deduced from the CHAMP/GPS satellite. J. Atmos. Sci. 61, 1610–1620, 2004.

Schmidt, T., de la Torre, A., Wickert, J. Global gravity wave activity in the tropopause region from CHAMP radio occultation data. Geophys. Res. Lett. 35, L16807, doi:10.1029/2008GL034986, 2008.

Senft, D.C., Hostetler, C.A., Gardner, C.S. Characteristics of gravity wave activity and spectra in the upper stratosphere and upper mesosphere at Arecibo during early April 1989. J. Atmos. Terr. Phys. 55, 425–439, 1993.

Smith, S.E., Fritts, D.C., VanZandt, T.E. Evidence of saturated spectrum of atmospheric gravity waves. J. Atmos. Sci. 44, 1404–1410, 1987.

Smith, R.B., Woods, B.K., Jensen, J., Cooper, W.A., Doyle, J.D., Jiang, Q., Grubisic, V. Mountain waves entering the stratosphere. J. Atmos. Sci. 65, 2543–2562, doi:10.1175/2007JAS2598.1, 2008.

Tsuda, T., VanZandt, T.E., Mizumoto, M., Kato, S., Fukao, S. Spectral analysis of temperature and Brunt–Väisälä frequency fluctuations observed by radiosondes. J. Geophys. Res. 96, 17265–17278, 1991.

Tsuda, T., Nishida, M., Rocken, C., Ware, R.H. A global morphology of gravity wave activity in the stratosphere revealed by the GPS

occultation data (GPS/MET). J. Geophys. Res. 105 (D6), 7257–7273, 2000.

VanZandt, T.E., Smith, S.A., Tsuda, T., Fritts, D.C., Sato, T., Fukao, S., Karo, S. Studies of velocity fluctuations in the lower atmosphere using the MU radar. Part I: azimuthal anisotropy. J. Atmos. Sci. 47, 39–50, 1990.

Wu, D.L., Waters, J.W. Satellite observations of atmospheric variances: a possible indication of gravity waves. Geophys. Res. Lett. 23, 3631–3634, 1996.

Wu, D.L., Preusse, P., Eckermann, S.D., et al. Remote sounding of atmospheric gravity waves with satellite limb and nadir techniques. Adv. Space Res. 37 (12), 2269–2277, 2006.